Gutzwiller wave-function solution for Anderson lattice model: Emerging universal regimes of heavy quasiparticle states

Marcin M. Wysokiński,[1,*] Jan Kaczmarczyk,[1,2,†] and Jozef Spałek[1,‡]

[1]*Marian Smoluchowski Institute of Physics, Jagiellonian University, ulica Łojasiewicza 11, PL-30-348 Kraków, Poland*

[2]*Institute of Science and Technology Austria, Am Campus 1, A-3400 Klosterneuburg, Austria*

(Received 26 May 2015; published 18 September 2015)

The recently proposed diagrammatic expansion (DE) technique for the full Gutzwiller wave function (GWF) is applied to the Anderson lattice model. This approach allows for a systematic evaluation of the expectation values with full Gutzwiller wave function in finite-dimensional systems. It introduces results extending in an essential manner those obtained by means of the standard Gutzwiller approximation (GA), which is variationally exact only in infinite dimensions. Within the DE-GWF approach we discuss the principal paramagnetic properties and their relevance to heavy-fermion systems. We demonstrate the formation of an effective, narrow f band originating from atomic f-electron states and subsequently interpret this behavior as a *direct itineracy* of f electrons; it represents a combined effect of both the hybridization and the correlations induced by the Coulomb repulsive interaction. Such a feature is absent on the level of GA, which is equivalent to the zeroth order of our expansion. Formation of the hybridization- and electron-concentration-dependent narrow f band rationalizes the common assumption of such dispersion of f levels in the phenomenological modeling of the band structure of $CeCoIn_5$. Moreover, it is shown that the emerging f-electron *direct itineracy* leads in a natural manner to three physically distinct regimes within a single model that are frequently discussed for $4f$- or $5f$-electron compounds as separate model situations. We identify these regimes as (i) the mixed-valence regime, (ii) Kondo/almost-Kondo insulating regime, and (iii) the Kondo-lattice limit when the f-electron occupancy is very close to the f-state half filling, $\langle \hat{n}_f \rangle \to 1$. The nonstandard features of the emerging correlated quantum liquid state are stressed.

DOI: 10.1103/PhysRevB.92.125135 PACS number(s): 71.27.+a, 71.28.+d, 71.10.Fd

I. INTRODUCTION AND MOTIVATION

Heavy-fermion systems (HFS) belong to the class of quantum materials with strongly correlated $4f$ or $5f$ electrons. They exhibit unique properties resulting from their universal electronic features (e.g., very high density of states at the Fermi level) almost independent of their crystal structure. Among those unique properties are (i) enormous effective masses in the Fermi-liquid state, as demonstrated through the linear specific-heat coefficient [1–5], and their direct spin dependence in the de Haas–van Alphen measurements [6–8], (ii) Kondo-type screening of localized or almost localized f-electron magnetic moments by the conduction electrons [9,10], (iii) unconventional superconductivity, appearing frequently at the border or coexisting with magnetism [11], and (iv) an abundance of quantum critical points and, associated with them, non-Fermi (non-Landau) liquid behavior [12–14].

The Anderson lattice model (ALM), also frequently referred to as the periodic Anderson model, and its derivatives, the Kondo [15–17] and the Anderson-Kondo [18,19] lattice models, capture the essential physics of HFS. Although the class of exact solutions is known for this model [20–23], the solutions are restricted in the parameter space. Thus, for thorough investigation of the model properties the approximate methods are needed. One of the earliest theoretical approaches for models with a strong Coulomb repulsion was the variational Gutzwiller wave-function (GWF) method [24–29]. However, despite its simple and physically transparent form, a direct analytic evaluation of the expectation values with full GWF cannot be carried out rigorously for arbitrary dimension and spatially unbound systems.

One of the ways to overcome this difficulty is the so-called Gutzwiller approximation (GA), in which only local two-particle correlations are taken into account when evaluating the expectation values. GA provides substantial insight into the overall properties of strongly correlated systems [9,10,26,30–35]. Moreover, this approach has been reformulated recently to the so-called *statistically consistent Gutzwiller approximation* (SGA) scheme and has been successfully applied to a number of problems involving correlated electron systems [19,36–43]. Among those, a concrete application has been the microscopic description of the fairly complete magnetic phase diagram of UGe_2 [42,43] which provided quantitatively correct results, even without taking into account the $5f$-orbital degeneracy due to uranium atoms.

An advanced method of evaluating the expectation values for GWF is the variational Monte Carlo technique (VMC) [44–52]. However, this method is computationally expensive and suffers from the system-size limitations. On the other hand, the VMC method allows for extension of GWF by including additional Jastrow factors [53].

Here we use an alternative method of evaluating the expectation values for GWF, namely, a systematic diagrammatic expansion for the Gutzwiller wave function (DE-GWF) [54–58]. This method was formulated initially for the Hubbard model in two dimensions in the context of Pomeranchuk instability [54] and was applied subsequently to the description of high-temperature superconductivity for the Hubbard [55,58] and the t-J [56] models. In the zeroth order of the expansion this approach straightforwardly reduces to the GA [56]. For the one-dimensional Hubbard model it converges [54] to the exact

*marcin.wysokinski@uj.edu.pl
†jan.kaczmarczyk@ist.ac.at
‡ufspalek@if.uj.edu.pl

GWF results. Within DE-GWF a larger variational space can be sampled than within the alternative VMC technique because the long-range components of the effective Hamiltonian are accounted for naturally. The DE-GWF method (truncated to match the variational spaces) reproduces the results of VMC with improved accuracy (as shown for the t-J [56] and Hubbard models [55]). Additionally, the method also works in the thermodynamic limit. In effect, the approach is well suited to capture subtle effects, e.g., those related to the topology of the Fermi surface in the correlated state [54] or the formation of a narrow f-electron band investigated herein.

In this study, we extend the DE-GWF approach to discuss the principal paramagnetic properties within ALM. The emergence of the quasiparticle picture is schematically illustrated in Fig. 1. Explicitly, we investigate the shape of the quasiparticle density of states (DOS) $\rho(E)$, which evolves with the increase of the order of the expansion k. For $k > 0$ the hybridization gap widens up with respect to that in GA ($k = 0$ case), and DOS peaks are significantly pronounced. Moreover, we investigate the evolution of the DOS at the Fermi level $\rho(E_F)$ on the hybridization strength-total-electron-concentration plane, $|V|$-n, as it is a direct measure of the heavy-quasiparticle effective mass. We find that this parameter is significantly enhanced for $k > 0$, mainly in the low hybridization limit and at the border of the Kondo-insulating state. Furthermore, we trace the contribution coming from the originally localized f electrons (see Fig. 1, top) to the quasiparticle spectrum with the increasing order of the expansion. For $k > 0$, f quasiparticles effectively acquire a nonzero bandwidth (up to 6% of the conduction bandwidth) as a combined effect of both interelectronic correlations and hybridization.

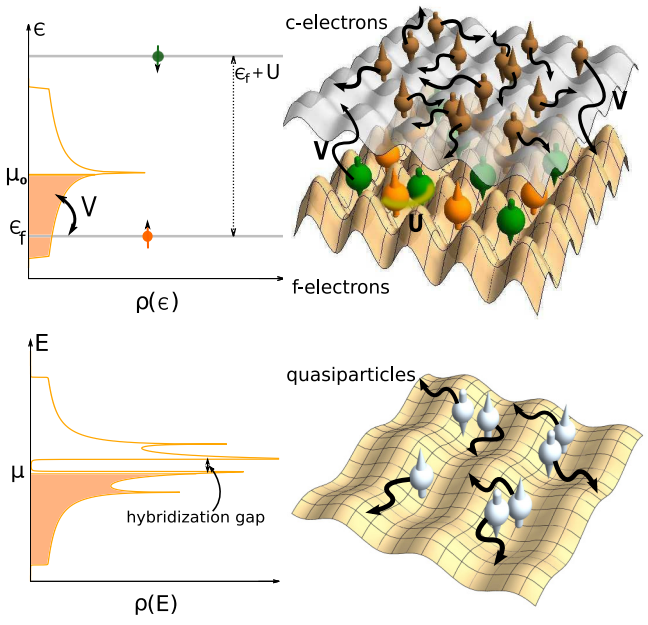

FIG. 1. (Color online) (top) Schematic representation of the two-orbital Anderson lattice model with initially localized f and delocalized c electrons and hybridization between them. (bottom) Emerging quasiparticle states in the hybridized bands of correlated particles. The left panel shows the shapes of the density of states in the respective situations.

The assumption of the existence of a narrow f band has recently been made in phenomenological modeling of the heavy-fermion compound $CeCoIn_5$ band structure [59–61]. We show that the emergence of such a band, absent in GA ($k = 0$), is evidence of the f-electron direct itineracy, which will be explained later. To quantify this itineracy we introduce the parameter w_f, the width of the effective, narrow f band. On the hybridization-strength–total-electron-concentration, $|V|$-n, plane, w_f is significantly enlarged in three distinct regimes, which we identify as the mixed-valence, Kondo/almost-Kondo insulating, and Kondo-lattice regimes (when the f-electron concentration is close to half filling, i.e., when $\langle \hat{n}_f \rangle \to 1$). These physically distinct regimes are frequently discussed and identified in various experiments [2,11,62–66] and in theory [19,33,67,68].

The structure of the paper is as follows. In Sec. II we describe the ALM Hamiltonian and define the Gutzwiller variational wave function in a nonstandard manner. In Sec. III we derive the DE-GWF method for ALM and determine the effective single-particle two-band Hamiltonian. In Sec. IV we present results concerning the paramagnetic properties: the quasiparticle spectrum, the resultant density of states at the Fermi level, and the formation of an effective narrow f-electron band out of initially localized states. In Appendix A we discuss the equivalence of the zeroth-order DE-GWF approach with GA. In Appendix B we present some technical details of the DE-GWF technique.

II. MODEL HAMILTONIAN AND GUTZWILLER WAVE FUNCTION

Our starting point is the ALM with the chemical potential μ, expressed through the Hamiltonian

$$\hat{\mathcal{H}} = \sum_{\mathbf{i},\mathbf{j},\sigma} t_{\mathbf{ij}} \hat{c}^{\dagger}_{\mathbf{i}\sigma} \hat{c}_{\mathbf{j}\sigma} - \sum_{\mathbf{i},\sigma} \mu \hat{n}^{c}_{\mathbf{i}\sigma} + \sum_{\mathbf{i},\sigma} (\epsilon_f - \mu) \hat{n}^{f}_{\mathbf{i}\sigma} + U \sum_{\mathbf{i}} \hat{n}^{f}_{\mathbf{i}\uparrow} \hat{n}^{f}_{\mathbf{i}\downarrow} + \sum_{\mathbf{i},\mathbf{j},\sigma} (V_{\mathbf{ij}} \hat{f}^{\dagger}_{\mathbf{i}\sigma} \hat{c}_{\mathbf{j}\sigma} + V^{*}_{\mathbf{ij}} \hat{c}^{\dagger}_{\mathbf{i}\sigma} \hat{f}_{\mathbf{j}\sigma}), \quad (1)$$

where $\mathbf{i} = (i_x, i_y)$ (and, similarly, $\mathbf{j}$) is the two-dimensional site index, $\hat{f}_{\mathbf{i}\sigma}$ ($\hat{f}^{\dagger}_{\mathbf{i}\sigma}$) and $\hat{c}_{\mathbf{i}\sigma}$ ($\hat{c}^{\dagger}_{\mathbf{i}\sigma}$) are the annihilation (creation) operators related to f and c orbitals, respectively, and $\sigma = \uparrow, \downarrow$ is the z-component direction of the spin. We assume that the hopping in the conduction band takes place between only the nearest-neighbor sites, $t_{\mathbf{ij}} \equiv t\delta_{|\mathbf{i}-\mathbf{j}|,1}$; the hybridization has the simplest on-site character [69], $V_{\mathbf{ij}} = V\delta_{\mathbf{i},\mathbf{j}}$; the local Coulomb repulsion on the f orbital has the amplitude U; and the initially atomic f states are located at the energy ϵ_f. In the following $|t|$ is used as the energy unit.

The GWF is constructed from the uncorrelated Slater determinant $|\psi_0\rangle$ by projecting out the fraction of the local double f occupancies by means of the Gutzwiller projection operator $\hat{P}_G$,

$$|\psi_G\rangle \equiv \hat{P}_G |\psi_0\rangle \equiv \prod_{\mathbf{i}} \hat{P}_{G;\mathbf{i}} |\psi_0\rangle. \quad (2)$$

In the GA approach when only a single f orbital (as in the present case) is correlated, the projection operator can be

defined by

$$\hat{P}_{G;\mathbf{i}} \equiv 1 - (1-g)\hat{n}^f_{\mathbf{i}\uparrow}\hat{n}^f_{\mathbf{i}\downarrow}, \tag{3}$$

where g is a variational parameter. Such a form allows for interpolating between the fully correlated ($g = 0$) and the uncorrelated ($g = 1$) limits. Equivalently, one can consider the average number of doubly occupied states, $\langle \hat{n}^f_{\mathbf{i}\uparrow}\hat{n}^f_{\mathbf{i}\downarrow}\rangle \equiv d^2$, as a variational parameter.

The Gutzwiller projection operator can be selected in a different manner as proposed in Ref. [70], namely,

$$\hat{P}^\dagger_{G;\mathbf{i}}\hat{P}_{G;\mathbf{i}} \equiv \hat{P}^2_{G;\mathbf{i}} = \mathbf{1} + x\hat{d}^{HF}_{\mathbf{i}}. \tag{4}$$

In the above relation x is a variational parameter, and for the paramagnetic and translationally invariant system we define Hartree-Fock (HF) operators of the form

$$\hat{d}^{HF}_{\mathbf{i}} \equiv \hat{n}^{HF}_{\mathbf{i}\uparrow}\hat{n}^{HF}_{\mathbf{i}\downarrow} = \left(\hat{n}^f_{\mathbf{i}\uparrow} - n_{0f}\right)\left(\hat{n}^f_{\mathbf{i}\downarrow} - n_{0f}\right), \tag{5}$$

where n_{0f} denotes the average occupation of a single f state and spin σ in the uncorrelated state $|\psi_0\rangle$, i.e., $n_{0f} = \langle \hat{f}^\dagger_{\mathbf{i}\sigma}\hat{f}_{\mathbf{i}\sigma}\rangle_0$. Hereafter shortened notation for the expectation values is used, i.e., $\langle\psi_0|\cdots|\psi_0\rangle \equiv \langle\cdots\rangle_0$. Strictly speaking, although $\hat{d}^{HF}_{\mathbf{i}}$ does not have the Hartree-Fock form of the double-occupancy operator, the HF superscript has its meaning as the property, $\langle\hat{d}^{HF}_{\mathbf{i}}\rangle_0 \equiv 0$ is preserved.

On the other hand, the Gutzwiller projection operator can be defined in general form as

$$\hat{P}_{G;\mathbf{i}} = \sum_\Gamma \lambda_\Gamma |\Gamma\rangle_{\mathbf{i}}\langle\Gamma|_{\mathbf{i}}, \tag{6}$$

with variational parameters $\lambda_\Gamma \in \{\lambda_0,\lambda_\uparrow,\lambda_\downarrow,\lambda_d\}$ that characterize the possible occupation probabilities for the four possible atomic Fock f states $|\Gamma\rangle_{\mathbf{i}} \in \{|0\rangle_{\mathbf{i}},|\uparrow\rangle_{\mathbf{i}},|\downarrow\rangle_{\mathbf{i}},|\uparrow\downarrow\rangle_{\mathbf{i}}\}$.

Relation (4) couples λ_Γ and x, reducing the number of independent variational parameters to one. Explicitly, we may express the parameters λ_Γ by the coefficient x,

$$\begin{aligned}
\lambda_0^2 &= 1 + xn_{0f}^2,\\
\lambda_\sigma^2 &= \lambda_{\bar{\sigma}}^2 \equiv \lambda_s^2 = 1 - xn_{0f}(1-n_{0f}),\\
\lambda_d^2 &= 1 + x(1-n_{0f})^2.
\end{aligned} \tag{7}$$

As the parameters λ_Γ and x are coupled by the conditions (7), there is freedom of choice of the variational parameter; in this work we have selected x. The parameter x covers the same variational space as g in GA. Additionally, the projector (4) leads to much faster convergence than (3) (cf. Ref. [54]). From (4) it is clear that $x = 0$ corresponds to the uncorrelated limit. The other extremity, the fully correlated state, is reached for $x = \max\{x(\lambda_d = 0), x(\lambda_0 = 0)\}$. This leads to the bounds $\max\{\frac{-1}{(1-n_{0f})^2}, \frac{-1}{(n_{0f})^2}\} \leqslant x \leqslant 0$. The minimal value is $x = -4$ for $n_{0f} = 0.5$.

This method is suitable for an arbitrary filling of the f orbital. However, because the present work mainly addresses the description of Ce-based compounds, we study the regime in which the f-orbital filling either does not exceed unity or is only slightly larger. Precisely, in the all figures presented here the f-orbital filling is never larger than 1.05.

III. DE-GWF METHOD

A. General scheme

In this section we present general implementation of the DE-GWF method. The procedure is composed of the following steps: (1) choice of the initial state $|\psi_0\rangle$, (2) evaluation of $\langle\hat{\mathcal{H}}\rangle_G \equiv \frac{\langle\psi_G|\hat{\mathcal{H}}|\psi_G\rangle}{\langle\psi_G|\psi_G\rangle}$ for selected $|\psi_0\rangle$ (see Sec. III B), (3) minimization of $\langle\hat{\mathcal{H}}\rangle_G$ with respect to the variational parameter (here x), (4) construction of the effective single-particle Hamiltonian determined by $\delta\hat{\mathcal{H}}^{\text{eff}}(|\psi_0\rangle) = \delta\hat{\mathcal{H}}(|\psi_0\rangle)$ (see Sec. III C), (5) determination of $|\psi_0'\rangle$ as a ground state of the effective Hamiltonian (see Sec. III D), and (6) execution of the self-consistent loop, starting again from step 1 with $|\psi_0'\rangle$ until a satisfactory convergence, i.e., $|\psi_0'\rangle = |\psi_0\rangle$, is reached. Steps 4 and 5 ensure that the final form of $|\psi_0\rangle$ represents the optimal choice which minimizes the ground-state energy $\langle\hat{\mathcal{H}}\rangle_G$. The DE-GWF method with respect to other related methods, GA and VMC, introduces a new technique for evaluating the expectation value of the correlated Hamiltonian with GWF (step 2 of the above procedure). In particular, it provides an important improvement because, e.g., for GA only single sites in the lattice contain the projection, whereas the remaining environment does not. GA leads, e.g., to the inability of obtaining the superconducting phase in the Hubbard model [55]. On the other hand, the VMC method tackles that problem properly, but at the price of extremely large computing power. This leads to the lattice size limitations (typically up to 20×20 sites) and a limited distance of real-space intersite correlations taken into account.

In this respect, DE-GWF introduces, in successive orders of the expansion, correlations to the environment of individual sites (beyond GA), and also converges in a systematic manner to the full GWF solution. Also, DE-GWF was shown to provide more accurate results than VMC [56] and, additionally, is free from the finite-size limitations. It also demands significantly less computational power than VMC. Thus, in general, this method is capable of treating more complex problems with GWF. On the other hand, DE-GWF is tailored specifically for GWF, while VMC allows for starting from different forms of the variational wave function, e.g., adding the Jastrow factors [52,53].

B. Diagrammatic expansion

The key point of the variational procedure is the calculation of the expectation value of Hamiltonian (1) with GWF $|\psi_G\rangle$ (point 1 from the scheme in Sec. III A) by starting from the expression

$$\langle\hat{\mathcal{H}}\rangle_G \equiv \frac{\langle\psi_G|\hat{\mathcal{H}}|\psi_G\rangle}{\langle\psi_G|\psi_G\rangle} = \frac{\langle\psi_0|\hat{P}_G\hat{\mathcal{H}}\hat{P}_G|\psi_0\rangle}{\langle\psi_0|\hat{P}_G^2|\psi_0\rangle}. \tag{8}$$

We use the DE-GWF technique [54–57] based on the expansion of the expectation values appearing in Eq. (8) in the power series in the variational parameter x, with the highest power representing the number of correlated vertices assumed to be correlated in the environment, except for local ones. This method is systematic in the sense that the zeroth order corresponds to GA [47], whereas the full GWF solution is approached as the order increases. Explicitly, we

determine the expectation values with respect to GWF of any product operator originating from the starting Hamiltonian (1) $\hat{\mathcal{O}}_{\mathbf{i(j)}} = \{\hat{c}^\dagger_{\mathbf{i}\sigma}\hat{c}_{\mathbf{j}\sigma}, \hat{n}^c_{\mathbf{i}\sigma}, \hat{n}^f_{\mathbf{i}\sigma}, \hat{n}^f_{\mathbf{i}\uparrow}\hat{n}^f_{\mathbf{i}\downarrow}, \hat{f}^\dagger_{\mathbf{i}\sigma}\hat{c}_{\mathbf{j}\sigma}, \hat{c}^\dagger_{\mathbf{i}\sigma}\hat{f}_{\mathbf{j}\sigma}\}$. This is executed by first accounting for the projection part on site $\mathbf{i}$ ($\mathbf{j}$), *external* vertices [e.g., computing $\hat{\mathcal{O}}^G_{\mathbf{i(j)}} \equiv \hat{P}_{G;\mathbf{i}}(\hat{P}_{G;\mathbf{j}})\hat{\mathcal{O}}_{\mathbf{i(j)}}(\hat{P}_{G;\mathbf{j}})\hat{P}_{G;\mathbf{i}}$; see below], and then including correlations (terms) to the other sites $\mathbf{l} \neq \mathbf{i},\mathbf{j}$, *internal* vertices, one by one.

Formally, the procedure starts with the effective power expansion in x of all relevant expectation values

$$\langle\psi_G|\hat{\mathcal{O}}_{\mathbf{i(j)}}|\psi_G\rangle = \left\langle \hat{\mathcal{O}}^G_{\mathbf{i(j)}} \prod_{\mathbf{l}\neq\mathbf{i},\mathbf{j}} \hat{P}^2_{G;l} \right\rangle_0 = \sum_{k=0}^{\infty} \frac{x^k}{k!} {\sum_{\mathbf{l}_1,\ldots,\mathbf{l}_k}}' \langle \hat{\mathcal{O}}^G_{\mathbf{i(j)}} \hat{d}^{HF}_{\mathbf{l}_1,\ldots,\mathbf{l}_k} \rangle_0, \tag{9}$$

where $\hat{d}^{HF}_{\mathbf{l}_1,\ldots,\mathbf{l}_k} \equiv \hat{d}^{HF}_{\mathbf{l}_1}\cdots\hat{d}^{HF}_{\mathbf{l}_k}$. The prime in the multiple summation denotes restrictions: $\mathbf{l}_p \neq \mathbf{l}_{p'}$, and $\mathbf{l}_p \neq \mathbf{i},\mathbf{j}$ for all p,p'. k is the order of the expansion. Note that for $k=0$ we obtain $\langle\psi_G|\hat{\mathcal{O}}_{\mathbf{i(j)}}|\psi_G\rangle = \langle\hat{\mathcal{O}}^G_{\mathbf{i(j)}}\rangle_0$. This means that the projection operators act only locally (i.e., only sites $\mathbf{i}$ and $\mathbf{j}$ are affected), and in this case we recover the GA results (for a detailed discussion of the equivalence see Appendix A). Expectation values in (9) can now be calculated by means of Wick's theorem in its real-space version because they involve only products averaged with $|\psi_0\rangle$. Such a power expansion in x allows for taking into account long-range correlations between k internal sites $(\mathbf{l}_1,\ldots,\mathbf{l}_k)$ and the external ones $(\mathbf{i},\mathbf{j})$. It must be noted that it is not a perturbative expansion with respect to the small parameter x. Instead, the expansion should be understood as an analytic series with the order determined by the number of correlated internal vertices taken in the nonlocal environment. For $k=\infty$, the full GWF solution would be obtained. However, on the basis of our results, satisfactory results for the expansion in the ALM case are already reached starting at $k=3$.

As noted above, the expectation values $\langle\cdots\rangle_0$ in Eq. (9) can be evaluated by means of Wick's theorem. Then, the terms with k internal sites can be visualized as diagrams with k internal and 1 (or 2) external vertices. The lines connecting those vertices are defined as

$$\begin{aligned} C_{\mathbf{ij}} &\equiv \langle\hat{c}^\dagger_{\mathbf{i}\sigma}\hat{c}_{\mathbf{j}\sigma}\rangle_0, \\ W_{\mathbf{ij}} &\equiv \langle\hat{f}^\dagger_{\mathbf{i}\sigma}\hat{c}_{\mathbf{j}\sigma}\rangle_0, \\ F_{\mathbf{ij}} &\equiv \langle\hat{f}^\dagger_{\mathbf{i}\sigma}\hat{f}_{\mathbf{j}\sigma}\rangle_0 - \delta_{\mathbf{ij}}n_{0f}. \end{aligned} \tag{10}$$

By constructing the projector operator (4), we have eliminated all the diagrams with the local f-orbital contractions ($\langle\hat{f}^\dagger_{\mathbf{i}\sigma}\hat{f}_{\mathbf{i}\sigma}\rangle_0$), the so-called *Hartree bubbles*. This procedure, as discussed explicitly in Ref. [54], leads to significantly faster convergence than that with the usual Gutzwiller projector, with the variational parameter g [71]. It constitutes the main reason for the efficiency of the DE-GWF method. Finally, all the expectation values with respect to GWF are normalized by $\langle\psi_G|\psi_G\rangle$ [see Eq. (8)]. However, through the linked-cluster theorem [72], the terms coming from expansion of $\langle\psi_G|\psi_G\rangle \equiv \langle\psi_0|\hat{P}^2_G|\psi_0\rangle$ cancel out with all disconnected diagrams appearing in the numerator of Eq. (8). In effect, the expectation values can be expressed in the closed form by the diagrammatic sums $S \in \{T^{cc(1,1)}_{\mathbf{ij}}, T^{fc(1,1)}, T^{fc(3,1)}, I^{c(2)}, I^{f(2)}, I^{f(4)}\}$, defined in Appendix B, which leads to the following resultant expression for the ground-state energy:

$$\begin{aligned} \frac{\langle\hat{\mathcal{H}}\rangle_G}{L} &= \frac{2}{L}\sum_{\mathbf{i},\mathbf{j}} t_{\mathbf{ij}} T^{cc(1,1)}_{\mathbf{ij}} - 2\mu I^{c(2)} \\ &\quad + 2(\epsilon_f - \mu)[n_{0f} + (1+xm)I^{f(2)} + \gamma I^{f(4)}] \\ &\quad + U\lambda_d^2[d_0 + 2n_{0f}I^{f(2)} + (1-xd_0)I^{f(4)}] \\ &\quad + 4V(\alpha T^{fc(1,1)} + \beta T^{fc(3,1)}), \end{aligned} \tag{11}$$

where the trivial sums $\sum_\sigma = 2$ and $\sum_{\mathbf{i}} = L$ have already been included. Parameters $\{\alpha,\beta,\gamma,m,d_0\}$ are all functions of n_{0f} and x [see Appendix B, Eq. (B2)]. For $k=0$, only the diagrammatic sums $T^{cc(1,1)}_{\mathbf{ij}}, I^{c(2)}$, and $T^{fc(1,1)}$ do not vanish, and we reproduce the standard GA result; the Coulomb energy reduces to $U\lambda_d^2 d_0$, and the hybridization reduces to $4V\alpha\langle\hat{f}^\dagger_{\mathbf{i}}\hat{c}_{\mathbf{i}}\rangle_0$, whereas the diagrammatic sums for the c band are only trivial (see the discussion in Appendix A).

The expectation value $\langle\hat{\mathcal{H}}\rangle_G$ calculated diagrammatically is minimized next with respect to the variational parameter x (step 3 in the scheme in Sec. III A).

C. Effective quasiparticle Hamiltonian

The next step in our procedure (step 4 in the scheme in Sec. III A) is mapping the correlations contained in $\langle\psi_G|\hat{\mathcal{H}}|\psi_G\rangle/\langle\psi_G|\psi_G\rangle$ onto the corresponding uncorrelated expectation value $\langle\psi_0|\hat{\mathcal{H}}^{\text{eff}}|\psi_0\rangle$. It is realized via the condition that the minima of the expectation values of both Hamiltonians coincide for the same equilibrium values of lines (10) and n_{0f}, which define $|\psi_0\rangle$. Note that the present formulation of this step of our minimization procedure is equivalent to those previously used [54–58]. Explicitly,

$$\begin{aligned} &\delta\langle\hat{\mathcal{H}}^{\text{eff}}\rangle_0(C,F,W,n_{0f}) \\ &\quad = \delta\langle\hat{\mathcal{H}}\rangle_G(C,F,W,n_{0f}) \\ &\quad = \frac{\partial\langle\hat{\mathcal{H}}\rangle_G}{\partial C}\delta C + \frac{\partial\langle\hat{\mathcal{H}}\rangle_G}{\partial W}\delta W + \frac{\partial\langle\hat{\mathcal{H}}\rangle_G}{\partial F}\delta F + \frac{\partial\langle\hat{\mathcal{H}}\rangle_G}{\partial n_{0f}}\delta n_{0f}, \end{aligned} \tag{12}$$

where skipping lattice indices for lines means that we consider each of them separately. This condition leads directly to the following form of the effective single-particle two-band Hamiltonian with nonlocal interband hybridization:

$$\hat{\mathcal{H}}^{\text{eff}} = \sum_{\mathbf{i},\mathbf{j},\sigma} t^c_{\mathbf{ij}}\hat{c}^\dagger_{\mathbf{i}\sigma}\hat{c}_{\mathbf{j}\sigma} + \sum_{\mathbf{i},\mathbf{j},\sigma} t^f_{\mathbf{ij}}\hat{f}^\dagger_{\mathbf{i}\sigma}\hat{f}_{\mathbf{j}\sigma} + \sum_{\mathbf{i},\mathbf{j},\sigma}(V^{fc}_{\mathbf{ij}}\hat{c}^\dagger_{\mathbf{i}\sigma}\hat{f}_{\mathbf{j}\sigma} + \text{H.c.}), \tag{13}$$

where the effective hopping and hybridization parameters are derivatives with respect to lines,

$$t^c_{\mathbf{ij}} = \frac{\partial\langle\hat{\mathcal{H}}\rangle_G}{\partial C_{\mathbf{ij}}}, \quad V^{fc}_{\mathbf{ij}} = \frac{\partial\langle\hat{\mathcal{H}}\rangle_G}{\partial W_{\mathbf{ij}}}, \quad t^f_{\mathbf{ij}} = \frac{\partial\langle\hat{\mathcal{H}}\rangle_G}{\partial F_{\mathbf{ij}}}, \quad t^f_{\mathbf{ii}} = \frac{\partial\langle\hat{\mathcal{H}}\rangle_G}{\partial n_{0f}}. \tag{14}$$

D. Determination of $|\psi_0'\rangle$

In this section we determine $|\psi_0'\rangle$ as a ground state of $\hat{\mathcal{H}}^{\rm eff}$ (step 5 of the scheme in Sec. III A).

In order to obtain the effective dispersion relations for c and f electrons and the $\mathbf{k}$-dependent hybridization we use the lattice Fourier transform

$$\epsilon_{\mathbf{k}}^{c(f)} = \frac{1}{L}\sum_{\mathbf{i},\mathbf{j}} e^{i(\mathbf{i}-\mathbf{j})\mathbf{k}} t_{\mathbf{ij}}^{c(f)},$$

$$V_{\mathbf{k}}^{cf} = \frac{1}{L}\sum_{\mathbf{i},\mathbf{j}} e^{i(\mathbf{i}-\mathbf{j})\mathbf{k}} V_{\mathbf{ij}}^{fc}. \tag{15}$$

In this manner, we reduce the many-body problem to the effective single-quasiparticle picture (see Fig. 1) described by the effective two-band Hamiltonian. The 2×2 matrix representation of Eq. (13) resulting from such a transform has the following form:

$$\hat{\mathcal{H}}^{\rm eff} = \sum_{\mathbf{k},\sigma} (\hat{c}_{\mathbf{k}\sigma}^{\dagger}\ \hat{f}_{\mathbf{k}\sigma}^{\dagger}) \begin{pmatrix} \epsilon_{\mathbf{k}}^{c} & V_{\mathbf{k}}^{cf} \\ V_{\mathbf{k}}^{cf} & \epsilon_{\mathbf{k}}^{f} \end{pmatrix} \begin{pmatrix} \hat{c}_{\mathbf{k}\sigma} \\ \hat{f}_{\mathbf{k}\sigma} \end{pmatrix}$$

$$= \sum_{\mathbf{k},\sigma} (\hat{c}_{\mathbf{k}\sigma}^{\dagger}\ \hat{f}_{\mathbf{k}\sigma}^{\dagger}) \mathcal{T}^{\dagger} \begin{pmatrix} E_{\mathbf{k}+} & 0 \\ 0 & E_{\mathbf{k}-} \end{pmatrix} \mathcal{T} \begin{pmatrix} \hat{c}_{\mathbf{k}\sigma} \\ \hat{f}_{\mathbf{k}\sigma} \end{pmatrix}, \tag{16}$$

where the eigenvalues $E_{\mathbf{k}\pm}$ of the above Hamiltonian are

$$E_{\mathbf{k}a} = \xi_{\mathbf{k}}^{+} + a\sqrt{(\xi_{\mathbf{k}}^{-})^2 + \left(V_{\mathbf{k}}^{cf}\right)^2}, \tag{17}$$

where $a \equiv \pm 1$ differentiate between the two hybridized bands. For convenience, we have defined

$$\xi_{\mathbf{k}}^{+} \equiv \frac{\epsilon_{\mathbf{k}}^{c} + \epsilon_{\mathbf{k}}^{f}}{2}, \quad \xi_{\mathbf{k}}^{-} \equiv \frac{\epsilon_{\mathbf{k}}^{c} - \epsilon_{\mathbf{k}}^{f}}{2}. \tag{18}$$

$\mathcal{T}$ in Eq. (16) is the unitary transformation matrix to the basis in which $\hat{\mathcal{H}}^{\rm eff}$ is diagonal, defined as

$$\mathcal{T} = \begin{pmatrix} u_{+} & u_{-} \\ u_{-} & -u_{+} \end{pmatrix}, \tag{19}$$

where

$$u_{\pm} = \sqrt{\tfrac{1}{2}\left(1 \pm \frac{\xi_{\mathbf{k}}^{-}}{\sqrt{(\xi_{\mathbf{k}}^{-})^2 + (V_{\mathbf{k}}^{cf})^2}}\right)}. \tag{20}$$

It is now straightforward to obtain the principal correlation functions (lines),

$$\begin{aligned} \langle \hat{c}_{\mathbf{k}\sigma}^{\dagger} \hat{c}_{\mathbf{k}\sigma} \rangle_0 &= u_{+}^2 \Theta(E_{\mathbf{k}+}) + u_{-}^2 \Theta(E_{\mathbf{k}-}), \\ \langle \hat{f}_{\mathbf{k}\sigma}^{\dagger} \hat{c}_{\mathbf{k}\sigma} \rangle_0 &= u_{+}u_{-}[\Theta(E_{\mathbf{k}+}) - \Theta(E_{\mathbf{k}-})], \\ \langle \hat{f}_{\mathbf{k}\sigma}^{\dagger} \hat{f}_{\mathbf{k}\sigma} \rangle_0 &= u_{-}^2 \Theta(E_{\mathbf{k}+}) + u_{+}^2 \Theta(E_{\mathbf{k}-}), \end{aligned} \tag{21}$$

where $\Theta(E)$ denotes the Heaviside step function and plays the role of an energy cutoff for respective quasiparticle band energies (17). Using the inverse Fourier transformation, we obtain self-consistent equations for lines and n_{0f},

$$C_{\mathbf{ij}} = \frac{1}{L}\sum_{\mathbf{k}a} \langle \hat{c}_{\mathbf{k}\sigma}^{\dagger} \hat{c}_{\mathbf{k}\sigma} \rangle_0\, e^{i(\mathbf{i}-\mathbf{j})\mathbf{k}},$$

$$W_{\mathbf{ij}} = \frac{1}{L}\sum_{\mathbf{k}a} \langle \hat{f}_{\mathbf{k}\sigma}^{\dagger} \hat{c}_{\mathbf{k}\sigma} \rangle_0\, e^{i(\mathbf{i}-\mathbf{j})\mathbf{k}},$$

$$F_{\mathbf{ij}} = \frac{1}{L}\sum_{\mathbf{k}a} \langle \hat{f}_{\mathbf{k}\sigma}^{\dagger} \hat{f}_{\mathbf{k}\sigma} \rangle_0\, e^{i(\mathbf{i}-\mathbf{j})\mathbf{k}},$$

$$n_{0f} = \frac{1}{L}\sum_{\mathbf{k}a} \langle \hat{f}_{\mathbf{k}\sigma}^{\dagger} \hat{f}_{\mathbf{k}\sigma} \rangle_0. \tag{22}$$

To determine the properties of the model, we solve in the self-consistent loop the system of Eqs. (14) and (22) [54–58] (step 6 in the scheme in Sec. III A).

Finally, the ground-state energy E_G is defined by

$$E_G = \langle \hat{\mathcal{H}} \rangle_G |_0 + Ln\mu, \tag{23}$$

where $\langle \hat{\mathcal{H}} \rangle_G |_0$ denotes the expectation value (11) of the starting Hamiltonian for the equilibrium values of the lines and the total number of particles is defined by $n \equiv 2\langle \hat{n}_{\mathbf{i}\sigma}^{f} + \hat{n}_{\mathbf{i}\sigma}^{c} \rangle_G$. The f-orbital filling is defined by $n_f \equiv 2\langle \hat{n}_{\mathbf{i}\sigma}^{f} \rangle_G$.

IV. RESULTS AND DISCUSSION

A. System description and technical remarks

In our analysis we consider a square, translationally invariant, and infinite ($L \to \infty$) lattice, with two orbitals (f and c) per site. The square-lattice consideration is justified by the common quasi-two-dimensional layered structure of f atoms in the elementary cell of many Ce-based heavy-fermion systems [2,11] for which our studies are relevant.

While proceeding with the diagrammatic expansion (DE), in principle, two approximations need to be made. First, only the lines (10) satisfying the relation $|\mathbf{i}-\mathbf{j}|^2 = (i_x - j_x)^2 + (i_y - j_y)^2 \leqslant 10$ are taken into account (i.e., we make a real-space cutoff; see Fig. 2). For comparison, in VMC lines farther than these connecting nearest-neighbor sites (more precisely, only the lines corresponding to the hopping-term range of the starting Hamiltonian) are only rarely taken into account [49,50]. From our numerical calculations it follows that the nearest- and the second-nearest-neighbor contractions compose the dominant contributions [see Fig. 7(b) below].

The second limitation in DE is the highest order of the expansion k taken into account. Starting at $k = 3$, the asymptotic behavior of some properties such as the DOS at

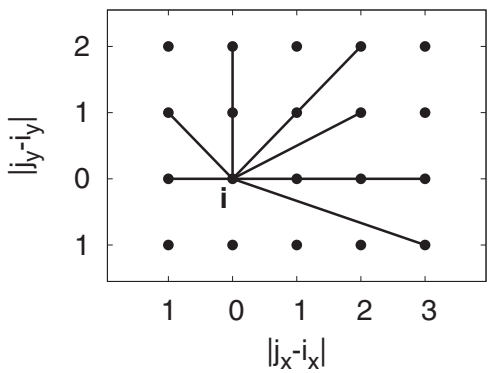

FIG. 2. Schematic illustration of the real-space cutoff on the lattice. The solid lines denote exemplary, in terms of distance, correlation functions (referred to as lines) taken into account between the $\mathbf{i}$ site (in the center) and the $\mathbf{j}$ sites (on the periphery). Farther connections are not considered.

the Fermi level $\rho(E_f)$ and the width of the effective f band w_f [see Figs. 4, 5(c), and 6 below] speak in favor of the calculation reliability, which has already been achieved in that order. Therefore, if not otherwise specified, the expansion is carried out up to the third order ($k = 3$), i.e., with the three internal vertices taken into account. We stress again that the zeroth-order approximation ($k = 0$) is equivalent to the GA approach (see Appendix A for details). The results of GA are regarded here as a reference point for determining a systematic evolution, including both qualitative and quantitative changes, when the higher-order contributions are implemented.

The parameters of the ALM Hamiltonian (1) are taken in units of $|t|$: a strong Coulomb repulsion is taken as $U = 10$, the reference energy for f electrons $\epsilon_f = -3$, the on-site hybridization is assumed to be negative and varies in the range $|V| \in (0.8, 2.5)$, and the total band filling ($n \equiv 2\langle \hat{n}^f_{i\sigma} + \hat{n}^c_{i\sigma} \rangle_G$) is in the range allowed by the condition that the f-level occupancy per site ($n_f \equiv 2\langle \hat{n}^f_{i\sigma} \rangle_G$) roughly does not exceed unity. The reason for considering this regime is the circumstance that for the Ce-based compounds that interest us the concentration of f electrons per cerium atom should not exceed 1 (i.e., with only the Ce^{3+} and Ce^{4+} configurations). However, from the construction of the method the regime for $n_f > 1$ is fully accessible and physically correct. In carrying out the DE-GWF procedure we adjust the chemical potential $\mu \equiv E_F$ for the fixed total filling n. Numerical integration of Eq. (22) and the self-consistent loop were both performed with precision of the order of 10^{-6} or better with the help of Gnu Scientific Library (GSL) procedures [73].

B. Correlated Fermi liquid

Before a detailed analysis is carried out, a methodological remark is needed. The effective Hamiltonian (13) is of single-particle form but coupled to the self-consistent procedure for evaluating the relevant averages (22). However, this does not compose the full picture. The physical quantities are those obtained with a projected wave function. For example, $n_f \equiv \sum_\sigma \langle \psi_G | \hat{f}^\dagger_{i\sigma} \hat{f}_{i\sigma} | \psi_G \rangle = \sum_\sigma \langle \mathcal{P}_G \hat{n}^f_{i\sigma} \mathcal{P}_G \rangle_0$, which, in general, is slightly different from $\sum_\sigma \langle \hat{n}^f_{i\sigma} \rangle_0$. The situation is illustrated explicitly in Fig. 3. In effect, the quasiparticle picture is amended with the nonstandard features of this *correlated* (*quantum*) *liquid* (CL). Parenthetically, the same difference will appear when considering magnetic and superconducting states, where the magnetic moments, $\langle \hat{S}^z_i \rangle_G$ vs. $\langle \hat{S}^z_i \rangle_0$, and the superconducting gaps, $\langle \hat{\Delta}_{ij} \rangle_G$ and $\langle \hat{\Delta}_{ij} \rangle_0$, will be different. Thus, we have a mapping of the correlated onto quasiparticle states but not of the physical properties. In brief, we have to distinguish between the correlated and uncorrelated f-electron occupancy or other property even though, from the way (13) was constructed, the density of quasiparticle states [coming from (13)] represents that in the correlated state.

C. Quasiparticle density of states

We start with an analysis of the quasiparticle DOS emerging from the DE-GWF method in successive orders of the expansion (see Fig. 4). For $k > 0$ and total filling $n = 1.97$ (i.e., near half filling), the hybridization peaks become more pronounced (see the table in the inset in Fig. 4), and the hybridization gap increases.

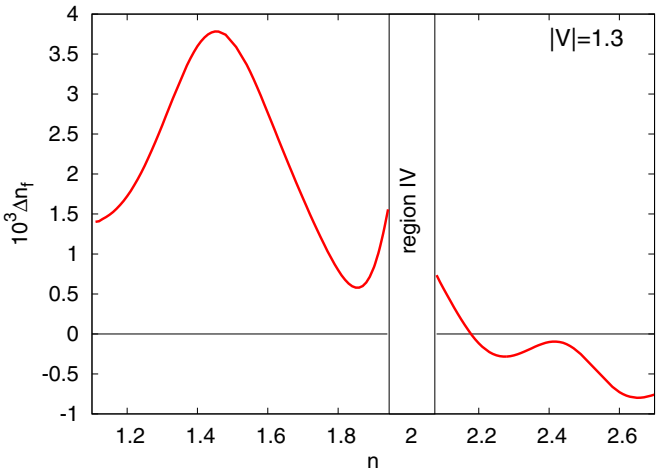

FIG. 3. (Color online) Difference between uncorrelated and correlated f-electron numbers, $\Delta n_f \equiv \sum_\sigma \langle \hat{n}^f_{i\sigma} \rangle_G - \sum_\sigma \langle \hat{n}^f_{i\sigma} \rangle_0$, along the line of constant hybridization, $|V| = 1.3$, with respect to changing total filling. The specific character of region IV is explained in Sec. IV.

For $k > 0$ the overall shape of DOS changes only quantitatively (see Fig. 4). However, the value of the DOS at the Fermi level $\rho(E_F)$ changes remarkably (see the inset in Fig. 4). Although it is underestimated for $k = 1$ and overestimated for $k = 2$, for $k = 4$ we see no significant difference with respect to the $k = 3$ case. For this reason, if not specified explicitly, the subsequent analysis is carried out in the third order, $k = 3$.

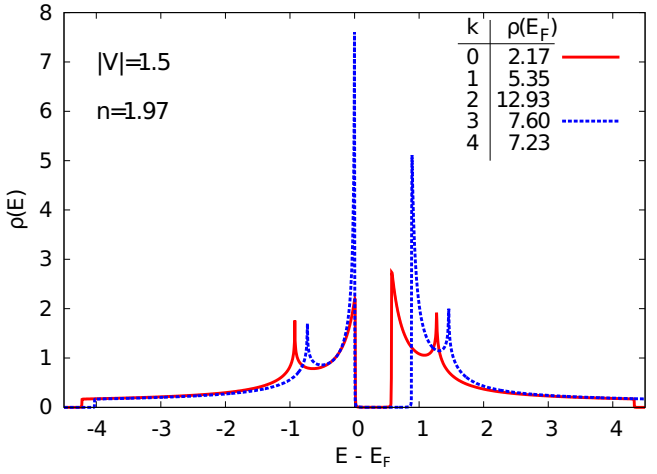

FIG. 4. (Color online) Density of states (DOS) near the half filling ($n = 1.97$) at $|V| = 1.5$ for selected orders of the diagrammatic expansion ($k = 0,3$). Explicit values of $\rho(E_F)$ are also listed in the inset table (for $0 \leqslant k \leqslant 4$). For $k = 3$ a satisfactory convergence of the expansion is reached. The $k = 1,2,4$ plots are not included for clarity because, apart from peak heights, they are practically the same as the plot for $k = 3$. For $k > 0$ (beyond GA) the hybridization peaks are more pronounced [large DOS at the Fermi level $\rho(E_F)$], which is related directly to the increased by correlation effective-mass enhancement for quasiparticles.

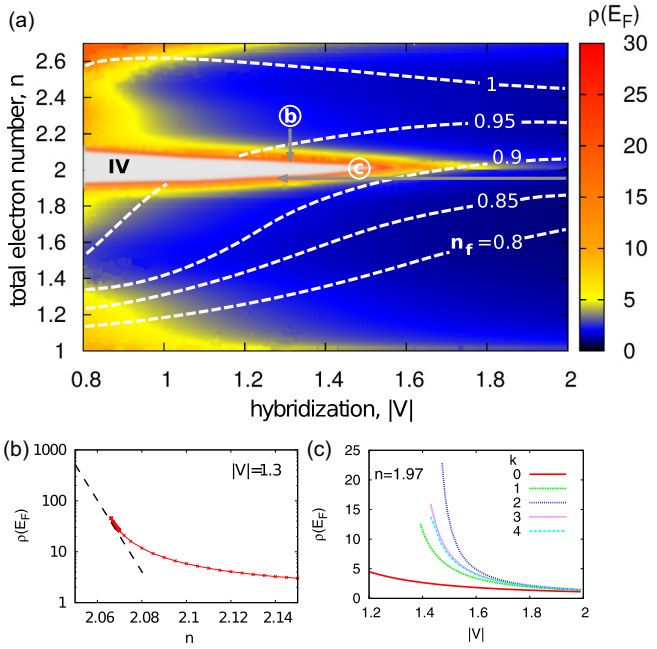

FIG. 5. (Color online) (a) Density of states at the Fermi level $\rho(E_F)$ on the hybridization-strength–total-electron-concentration plane, $|V|$-n. Additionally (not marked), for $n = 2$ we always obtain the Kondo insulating state. By region IV (labeled for consistency with Fig. 7) we have marked a V-shaped region where we have no numerical convergence due to the presence of singular hybridization peaks for low $|V|$ and with n near half filling (see main text). (b) Evolution of $\rho(E_F)$ in the half-logarithmic scale near region IV [along the vertical arrow labeled (b) in (a)]. By extrapolation [dashed line in (b)], for the almost-half-filled situation, $\rho(E_F)$ can even be enhanced by a factor of 1000 relative to its lowest values on the $|V|$-n plane. (c) Evolution of $\rho(E_F)$ with decreasing $|V|$ [along the horizontal arrow labeled (c) in (a)], within successive orders of the expansion ($k \leqslant 4$). For large $|V| \gtrsim 1.8$, GA ($k = 0$ order) provides realistic values of $\rho(E_F)$.

The value of $\rho(E_F)$ is of crucial importance. This parameter is a measure of the quasiparticle effective mass, as the latter is inversely proportional to the second derivative of the energy $\nabla^2_{\mathbf{k}} E_{\mathbf{k}}$ at the Fermi surface and thus is determined by $\rho(E_F)$.

In Fig. 5(a) we draw the value of $\rho(E_F)$ on the hybridization–total-electron-number (per site) plane, V-n. This quantity is particularly strongly enhanced near half filling ($n \simeq 2$). In comparison to the lowest value $\rho(E_F) \approx 0.75$, the maximal enhancement is of the order of 40. In Fig. 5(b) we present the evolution of $\rho(E_F)$ on the logarithmic scale as total filling decreases and approaches $n = 2$ (vertical arrow in Fig. 5(a) marked (b)]. The extrapolated value of $\rho(E_F)$ may reach the extremely high value of 1000 or even greater [dashed line in Fig. 5(b)] in region IV. Such a feature could explain extremely the high mass renormalization in some HFS for a large but finite value of the Coulomb interaction U.

The region where $\rho(E_F)$ is enhanced strongly is that with low hybridization $|V|$ values and for total filling $n \simeq 1$. This region is strictly correlated with the position of the second pronounced peak in DOS (see Fig. 4), which therefore has the meaning of the Van Hove singularity. Additionally, for $n_f \simeq 1$, where the effects of correlations are the strongest, we also observe a large value of $\rho(E_F)$. In that limit the stability of magnetic phases should be studied separately [18,19].

As marked in Fig. 5(a), near the total half filling, $n \simeq 2$, we could not obtain a satisfactory convergence of our self-consistent procedure. This is attributed to the position of the chemical potential extremely close to the hybridization-induced peaks (significant when $n_f \gtrsim 0.9$). Technically, this leads to extreme fluctuations (out of our numerical precision) of the filling, effective hopping parameters, and the lines coming from the effective Hamiltonian (13), as they are sensitive to a slight change in the chemical-potential position. For $n = 2$ and nonzero hybridization, we always obtain the Kondo-insulating state. However, strictly speaking, the true Kondo-type compensated state is demonstrated explicitly only if magnetic structure is taken into account explicitly [9,10,18].

In Fig. 5(c) we depict the $\rho(E_F)$ evolution with decreasing hybridization amplitude $|V|$ for $k \leqslant 4$. Our results show that for large $|V|$, GA ($k = 0$) already is a reasonable approximation. The situation changes as we approach the low-$|V|$ regime near half filling, where inclusion of higher-order contributions leads to a strong enhancement of $\rho(E_F)$, as discussed above.

In summary, the quasiparticle mass is enhanced significantly near $n = 2$ and in the regime of small hybridization $|V|$. The f-state occupancy is then $n_f \gtrsim 0.9$. This is the regime associated with the heavy-fermion and Kondo-insulating states. We discuss those states in detail below.

D. f-electron direct itineracy

As stated already, the DE-GWF method is used here to map the correlated (many-body) system, described by the original Hamiltonian (1) with the help of the Gutzwiller wave function $|\psi_G\rangle$, onto that described by the effective quasiparticle Hamiltonian (13) with an uncorrelated wave function $|\psi_0\rangle$. By constructing the effective Hamiltonian it is possible to extract the explicit contribution to the quasiparticle picture that comes from a direct hopping between the neighboring f sites. By contrast, in the GA ($k = 0$) case, the f-electron itineracy is only due to the admixture of c states when the quasiparticle states are formed. Once we proceed with the diagrammatic expansion to higher order ($k > 0$), they start contributing to the quasiparticle spectrum in the form of a dispersive f band (see Fig. 6). The resulting band is narrow, $w_f \leqslant 0.5$, whereas the starting conduction (c) band has a width of $w_c = 8$. As was mentioned in Sec. I, we interpret the parameter w_f as a measure of the emerging degree of *direct itineracy*, i.e., the presence of direct hoppings between the neighboring f states in the effective Hamiltonian.

Again, a methodological remark on the numerical convergence of the results with respect to k is needed. Namely, the f-bandwidth already appears for $k = 1$, but both its width and the curvature stabilize only from $k = 3$.

In the recent phenomenological modeling of $CeCoIn_5$ [59–61] the band structure used was the hybridized-two-band independent-particle model with a dispersive f band, even though the Ce $4f$ states can be placed well above the so-called Hill limit, where no direct hopping between the original neighboring f states should exist. The fit presented there gives w_f of the same order of magnitude as that obtained here. As those phenomenological models do not include the Coulomb

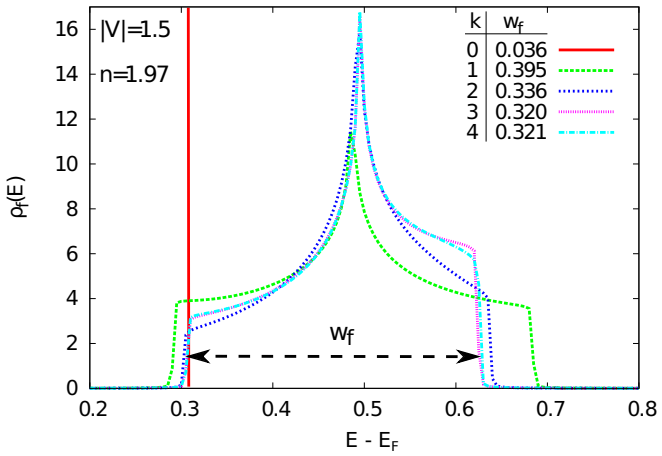

FIG. 6. (Color online) The f-electron density of states $\rho_f(E)$ within successive orders of expansion ($k \leqslant 4$). For $k = 1$ and higher, formation of the effective f band can be clearly observed. For $k = 3$ the final shape of $\rho_f(E)$ and the value of the f-band width w_f stabilize.

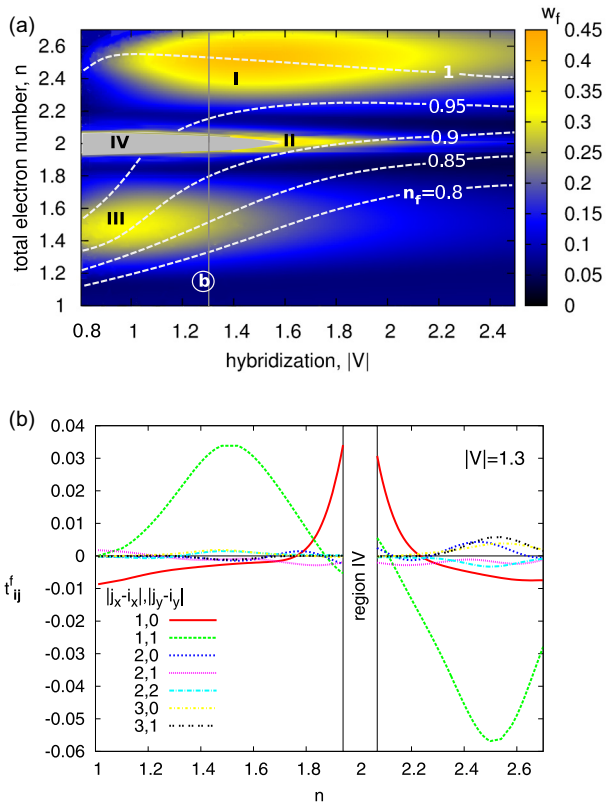

FIG. 7. (Color online) (a) Effective bandwidth of f states w_f on the hybridization-strength–electron-concentration plane, $|V|$-n. w_f is regarded as a measure of the direct itineracy of f-electron states. Three separate disjoint regions (light color) are regarded as universal and frequently discussed as separate limits, both in theory and experiment, namely, the mixed-valence regime (III), the Kondo/almost-Kondo insulating regime (II), and the Kondo-lattice regime (I) with $n_f \to 1 - \delta, \delta \ll 1$. (b) Effective f-electron intersite hoppings $t_{\mathbf{ij}}^f$ along the marked vertical line in (a) for $|V| = 1.3$. The energy dispersion for f quasiparticles is determined mainly by the nearest and the second-nearest hoppings $t_{\mathbf{ij}}^f$. Region IV, near $n = 2$, is marked separately due to the lack of convergence of the numerical results (see main text).

interaction, the ground state is determined with the uncorrelated wave function. Hence, our analysis of the effective Hamiltonian resulting from ALM provides a direct microscopic rationalization of the narrow dispersive f-band presence assumed *ad hoc* in the fitting procedure in Refs. [59–61].

In Fig. 7(a) we display a diagram comprising the width of the f band w_f on the $|V|$-n plane, with contours with constant values of n_f. We observe the appearance of some regions where the f quasiparticles have a sizable bandwidth (bright color) and others where they remain localized (dark regimes). We expect that in the regions where the f electrons are forming a band, nontrivial unconventional superconductivity and/or magnetism may appear. These topics should be treated separately as they require a substantial extension of the present approach (incorporating a new type of lines) [55–58].

With the help of the width w_f we may single out three physically distinct regimes [see Fig. 7(a)]. We identify those regions as the mixed-valence regime (III), the Kondo/almost-Kondo insulating regime (II), and the Kondo-lattice regime (I) with $n_f \to 1 - \delta$, with $\delta \ll 1$ [see Fig. 7(a)]. These universal regions are usually discussed independently within different specific models and methods. In regime I the role of f-c Coulomb interactions (the Falicov-Kimball term) may be needed for completeness (cf. Ref. [74]), whereas in the Kondo-lattice regime the transformation to the Anderson-Kondo model is appropriate (cf. Refs. [18,19]). In the extreme situation, the heavy-fermion states are modeled with a pure Kondo-lattice model [75–77]. However, strictly speaking, the last model applies only in the limit of localized f electrons ($n_f = 1$) since the total numbers of f and c electrons are conserved separately.

In Fig. 7(b) we present the effective hopping parameters for f states for $|V| = 1.3$, i.e., along the vertical line marked in Fig. 7(a). This line crosses three regions of the itineracy. The leading contribution to the f-electron band energy arises from the nearest- and the second-nearest-neighbor hoppings. This outcome confirms that our earlier assumption about the real-space cutoff shown in Fig. 2 has been selected properly. Moreover, it points to the importance of including the components beyond those of the starting Hamiltonian, which are only rarely taken into account within the VMC method [49,50].

In Fig. 8 we show the contributions to the effective hybridization. The initial (bare) local hybridization acquires momentum dependence. Nevertheless, the local part is still dominant since the nonlocal terms are at least two orders of magnitude smaller.

The emerging in our model f band introduces a new definition of the f-electron itineracy because it is not connected so much to the Fermi-surface size [78], but rather to the appearance of direct hoppings between f sites. This difference is highly nontrivial, especially in the limit $n_f = 1$, where we obtain the largest bandwidth w_f. Such behavior is attributed to the specific character of our approach. Namely, we consider here the processes within our initial Hamiltonian (1), but under the assumption that the neighboring sites are also correlated.

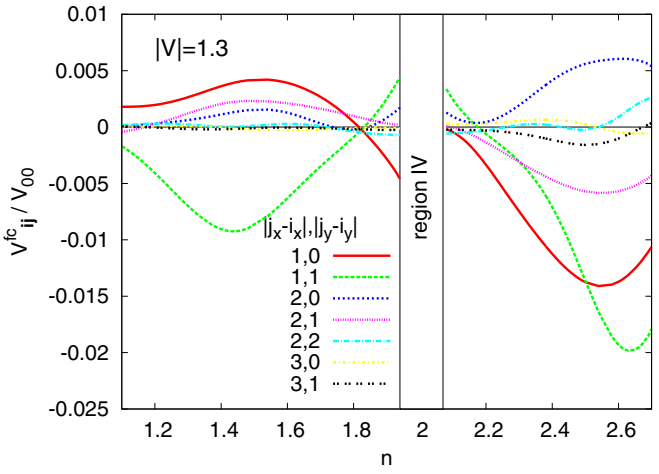

FIG. 8. (Color online) Spatial contributions $V^{cf}_{\mathbf{ij}}$ to the effective hybridization normalized by the first on-site ($\mathbf{i}=\mathbf{j}$) V_{00} term along the vertical line in Fig. 7(a) for $|V|=1.3$. Note that due to correlation initially local, on-site hybridization effectively acquires momentum dependence. However, the nonlocal contributions constitute only up to 2% of the local one.

This, as we have shown directly, also leads to the finite f band in the effective single-particle Hamiltonian (13). The results thus throw new light on the longstanding issue of the dual localized-itinerant nature of f electrons in HFS [79,80]. While the magnetism can be attributed to the almost localized nature of f electrons, unconventional superconductivity requires their itineracy in an explicit manner, which will be discussed elsewhere [81].

V. SUMMARY

We have applied a recently developed diagrammatic technique (DE-GWF) for evaluating the expectation values with the full Gutzwiller wave function for the case of a two-dimensional Anderson lattice. We have analyzed the properties of the model by discussing the most important features of the heavy-fermion systems in the paramagnetic state. We have also shown that by approaching the full Gutzwiller-wave-function solution in successive orders of the expansion, we obtain a systematic convergence. In the zeroth order of the expansion our method reduces to the standard Gutzwiller approximation.

In contrast to GA, DE-GWF does not overestimate the hybridization narrowing factor. Furthermore, our method produces unusually enhanced peaks at the Fermi level in the density of states, particularly near the half filling, $n \to 2$. This, in turn, is connected to the value of the effective mass, and by analyzing this region in detail we can explain the very large mass enhancement observed in heavy-fermion systems as described by ALM with a large, but finite, Coulomb-interaction value, here $U = 10|t|$. The regions with sizable $\rho(E_F)$ enhancement are also found in the small-hybridization limit and are connected to the presence of both the Van Hove singularity and strong correlations in the limit of $n_f \to 1$.

The f-electron contribution to the full quasiparticle spectrum has been analyzed in detail. For nonzero order of the expansion ($k > 0$) we observe a systematic formation of the effective f band with increasing k. Although the bare electrons are initially localized, f quasiparticles contribute to the total density of states as they become itinerant. We interpret this property as the emerging direct f-electron itineracy. As a measure of this behavior, we introduce the the width w_f of the effective f band. The formation of such a narrow f band rationalizes, e.g., the recent phenomenological modeling of the $CeCoIn_5$ band structure [59–61].

The nonstandard character of the resultant correlated Fermi liquid (FL), which differs from both the Landau FL and the spin liquid (SL), should be stressed. The FL represents a weakly correlated state (no localization), and the SL represents a fully correlated state. Our CL state has an intermediate character in this respect. Namely, the quasiparticle states are formed (as exemplified by, e.g., the density of states), but the physical properties such as the occupancy n_f, the magnetic moment $\langle \hat{S}^z_{\mathbf{i}} \rangle$, and the pairing gap in real space $\langle \hat{\Delta}_{\mathbf{ij}} \rangle$ are strongly renormalized by the correlations. Such a situation is often called an almost-localized Fermi-liquid state [4,9,10,16,17].

By analyzing the results on the hybridization-strength–total-band-filling plane, $|V|$-n, we single out explicitly three physically distinct regions, which we regard as three separate universality limits. Namely, we have linked those disjoint regions with the regimes frequently discussed as separate classes in heavy-fermion systems: the mixed-valence regime, the Kondo/almost-Kondo insulating regime, and the Kondo-lattice regime for $n_f \to 1$. We suggest that the regions of significant f-electron itineracy can be connected to the unconventional heavy-fermion superconductivity, which requires separate studies.

We have also commented on the longstanding issue of the dual localized-itinerant nature of f electrons in heavy-fermion systems. Our definition of itineracy is in agreement with their (almost) localized nature.

ACKNOWLEDGMENTS

We are grateful for discussions with J. Bünemann. The work was partly supported by the National Science Centre (NCN) under MAESTRO, Grant No. DEC-2012/04/A/ST3/00342. Access to the supercomputer located at the Academic Center for Materials and Nanotechnology of the AGH University of Science and Technology in Kraków is also acknowledged. M.W. acknowledges the hospitality of the Institute of Science and Technology Austria during the final stage of development of the present work, as well as partial financial support from the Society-Environment-Technology project of the Jagiellonian University for that stay. J.K. acknowledges support from the People Programme (Marie Curie Actions) of the European Union's Seventh Framework Programme (FP7/2007-2013) under REA Grant Agreement No. [291734].

APPENDIX A: EQUIVALENCE OF THE $k = 0$ ORDER DE-GWF EXPANSION AND THE GUTZWILLER APPROXIMATION

Here we show the equivalence of the zeroth-order DE-GWF and the standard Gutzwiller approximation (GA). In both methods (DE-GWF in the zeroth order of expansion $k = 0$) the effect of the projection can be summarized by the expressions

for evaluating the following expectation values: $\langle \hat{n}_{\mathbf{i}\uparrow}\hat{n}_{\mathbf{i}\downarrow}\rangle_G$ and $\langle \hat{f}^\dagger_{\mathbf{i}\sigma}\hat{c}_{\mathbf{i}\sigma} + \text{H.c.}\rangle_G$. The remaining averages in ALM are unchanged under the projection.

Explicitly, in the DE-GWF for $k = 0$ the resulting averages are expressed as follows:

$$\langle \hat{n}_{\mathbf{i}\uparrow}\hat{n}_{\mathbf{i}\downarrow}\rangle_G^{(k=0)} = \lambda_d^2 n_{0f}^2, \tag{A1a}$$

$$\langle \hat{f}^\dagger_{\mathbf{i}\sigma}\hat{c}_{\mathbf{i}\sigma} + \text{H.c.}\rangle_G^{(k=0)} = \alpha\langle \hat{f}^\dagger_{\mathbf{i}\sigma}\hat{c}_{\mathbf{i}\sigma} + \text{H.c.}\rangle_0, \tag{A1b}$$

where α [see also Appendix B, Eqs. (B1) and (B2)] is defined as

$$\alpha \equiv (1 - n_{0f})\lambda_0\lambda_s + n_{0f}\lambda_d\lambda_s. \tag{A2}$$

On the other hand, in GA the resulting averages are expressed as [26]

$$\langle \hat{n}_{\mathbf{i}\uparrow}\hat{n}_{\mathbf{i}\downarrow}\rangle_G^{(GA)} = \langle n^f_{\mathbf{i}\uparrow}\hat{n}^f_{\mathbf{i}\downarrow}\rangle_0 \equiv d^2, \tag{A3a}$$

$$\langle \hat{f}^\dagger_{\mathbf{i}\sigma}\hat{c}_{\mathbf{i}\sigma} + \text{H.c.}\rangle_G^{(GA)} = \sqrt{q}\langle \hat{f}^\dagger_{\mathbf{i}\sigma}\hat{c}_{\mathbf{i}\sigma} + \text{H.c.}\rangle_0, \tag{A3b}$$

where d^2 is the double-occupancy probability and q is the so-called Gutzwiller factor reducing the hybridization amplitude, which for an equal number of particles for each spin is defined as

$$\sqrt{q} = \frac{\sqrt{(n_{0f} - d^2)(1 - 2n_{0f} + d^2)} + \sqrt{(n_{0f} - d^2)d^2}}{\sqrt{n_{0f}(1 - n_{0f})}}. \tag{A4}$$

If we identify double-occupancy probabilities expressed by both methods in (A3a) and (A1a) to be equal, yielding $d^2 = \lambda_d^2 n_{0f}^2$, then α in (A2) exactly reduces to $\sqrt{q}$ in (A4).

GA procedure results in the effective single-particle Hamiltonian of the form

$$\hat{\mathcal{H}}_{GA} \equiv \sum_{\mathbf{k},\sigma} \hat{\Psi}^\dagger_{\mathbf{k}\sigma} \begin{pmatrix} \epsilon^c_{\mathbf{k}} - \mu & \sqrt{q_\sigma}V \\ \sqrt{q_\sigma}V & \epsilon_f - \mu \end{pmatrix} \hat{\Psi}_{\mathbf{k}\sigma} + LUd^2 - \lambda^f_n\left(\sum_{\mathbf{k},\sigma}\hat{n}^f_{\mathbf{k},\sigma} - Ln_{0f}\right) - \lambda^f_m\left(\sum_{\mathbf{k},\sigma}\sigma\hat{n}^f_{\mathbf{k},\sigma} - Lm_f\right). \tag{A5}$$

In the above Hamiltonian it is necessary to add constraints for the number and the magnetization of f electrons in order to satisfy consistency of the procedure [27,82]. In effect, the whole variational problem is reduced to minimization of the ground-state energy with respect to d^2, n_{0f}, m_f, and the respective Lagrange multipliers λ^f_n and λ^f_m, which play the role of the effective molecular fields [82]. However, the effect of a constraint on f-electron magnetization is relevant only when magnetism is intrinsic [42,43] or induced by applied magnetic field [41]. Here the paramagnetic state $m^f = \lambda^f_m = \lambda^f_n = 0$.

The DE-GWF method, by construction, guarantees that the variationally obtained f-electron occupancy number n_f coincides with that obtained self-consistently [57]. We have thus provided an analytical argument for the equivalence of the DE-GWF method for $k = 0$ and the standard GA procedure. Also, using an independent numerical cross-check, we have verified that all the observables calculated within both methods indeed coincide.

APPENDIX B: DIAGRAMMATIC SUMS

We start with expressions for the following projected operators originating from the ALM Hamiltonian (1):

$$\begin{aligned} \hat{P}_{G;\mathbf{i}}\hat{d}_{\mathbf{i}}\hat{P}_{G;\mathbf{i}} &= \lambda_d^2\left[2n_{0f}\hat{n}^{HF}_{\mathbf{i}} + (1 - xd_0)\hat{d}^{HF}_{\mathbf{i}} + d_0\hat{P}^2_{G;\mathbf{i}}\right], \\ \hat{P}_{G;\mathbf{i}}\hat{n}_{\mathbf{i}\sigma}\hat{P}_{G;\mathbf{i}} &= (1 + xm)\hat{n}^{HF}_{\mathbf{i}} + \gamma\hat{d}^{HF}_{\mathbf{i}} + n_{0f}\hat{P}^2_{G;\mathbf{i}}, \\ \hat{P}_{G;\mathbf{i}}\hat{f}^{(\dagger)}_{\mathbf{i}\sigma}\hat{P}_{G;\mathbf{i}} &= \alpha\hat{f}^{(\dagger)}_{\mathbf{i}\sigma} + \beta\hat{f}^{(\dagger)}_{\mathbf{i}\sigma}\hat{n}^{HF}_{\mathbf{i}}, \end{aligned} \tag{B1}$$

where, additionally, we have defined

$$\begin{aligned} \hat{n}^{HF}_{\mathbf{i}} &\equiv \hat{n}^{HF}_{\mathbf{i}\sigma} = \hat{n}^{HF}_{\mathbf{i}\bar{\sigma}}, \\ \beta &\equiv \lambda_s(\lambda_d - \lambda_0), \\ \alpha &\equiv \lambda_s\lambda_0 + \beta n_{0f}, \\ \gamma &\equiv x(1 - 2n_{0f}), \\ d_0 &\equiv n_{0f}^2, \\ m &\equiv n_{0f}(1 - n_{0f}). \end{aligned} \tag{B2}$$

As mentioned in the main text, such a form of the projected operators significantly speeds up the convergence of the numerical results [54] since by construction all two-operator averages for a single site and f orbital, the so-called *Hartree bubbles*, vanish. The above operator algebra

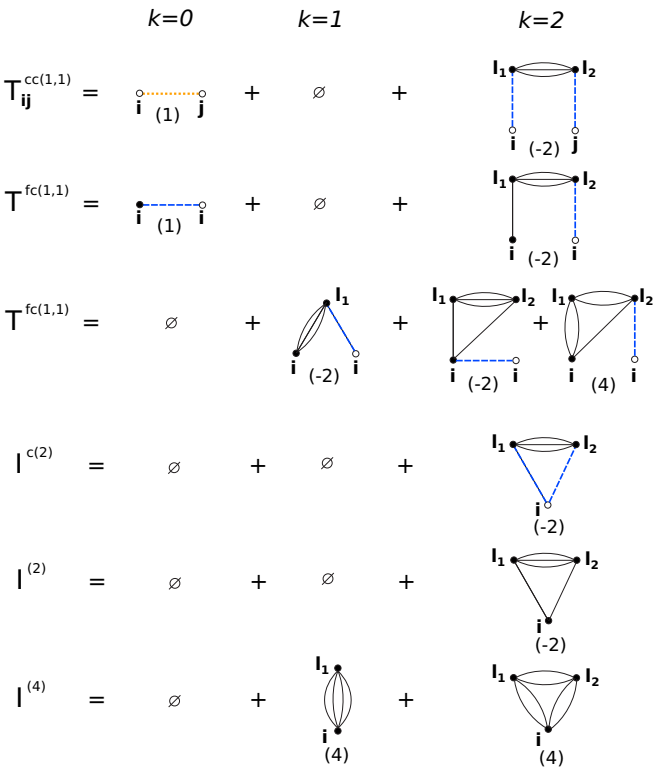

FIG. 9. (Color online) Diagrammatic sums to the second order, $k = 2$. The c- and f-orbital sites are denoted with empty and solid circles, respectively. Solid black, dashed blue, and dotted orange connections represent F, W, and C lines, respectively [see Eq. (10)]. The numbers in parentheses under the diagrams indicate their multiplicity resulting from Wick's theorem. Note that by construction of our sums we have no diagrams with so-called Hartree bubbles, namely, loop lines within the same site and orbital.

leads to the compact definition of the diagrammatic sums, $S \in \{T_{\mathbf{ij}}^{cc(1,1)}, T_{\mathbf{ij}}^{fc(1,1)}, T_{\mathbf{ij}}^{fc(3,1)}, I^{c(2)}, I^{(2)}, I^{(4)}\}$ in Eq. (11),

$$S = \sum_{k=0}^{\infty} \frac{x^k}{k!} S(k), \tag{B3}$$

with the kth-order contributions

$$T_{\mathbf{ij}}^{cc(1,1)}(k) \equiv \sum_{\mathbf{l}_1,\ldots,\mathbf{l}_k} \langle \hat{c}_{\mathbf{i}\sigma}^{\dagger} \hat{c}_{\mathbf{j}\sigma} \hat{d}_{\mathbf{l}_1,\ldots,\mathbf{l}_k}^{HF} \rangle_0^c,$$

$$T^{fc(1[3],1)}(k) \equiv \sum_{\mathbf{l}_1,\ldots,\mathbf{l}_k} \langle [\hat{n}_{\mathbf{i}}^{HF}] \hat{f}_{\mathbf{i}\sigma}^{\dagger} \hat{c}_{\mathbf{i}\sigma} \hat{d}_{\mathbf{l}_1,\ldots,\mathbf{l}_k}^{HF} \rangle_0^c,$$

$$I^{c(2)}(k) \equiv \sum_{\mathbf{l}_1,\ldots,\mathbf{l}_k} \langle \hat{n}_{\mathbf{i}\sigma}^{c} \hat{d}_{\mathbf{l}_1,\ldots,\mathbf{l}_k}^{HF} \rangle_0^c,$$

$$I^{(2)}(k) \equiv \sum_{\mathbf{l}_1,\ldots,\mathbf{l}_k} \langle \hat{n}_{\mathbf{i}}^{HF} \hat{d}_{\mathbf{l}_1,\ldots,\mathbf{l}_k}^{HF} \rangle_0^c,$$

$$I^{(4)}(k) \equiv \sum_{\mathbf{l}_1,\ldots,\mathbf{l}_k} \langle \hat{d}_{\mathbf{i}}^{HF} \hat{d}_{\mathbf{l}_1,\ldots,\mathbf{l}_k}^{HF} \rangle_0^c. \tag{B4}$$

A superscript c in the expectation values means that only the connected diagrams should be included. Note that in (B4) there are no summation restrictions due to the linked cluster theorem [72]. The resulting diagrammatic sums for S up to second order ($k = 2$) are depicted in Fig. 9.

[1] K. Andres, J. E. Graebner, and H. R. Ott, Phys. Rev. Lett. **35**, 1779 (1975).
[2] G. R. Stewart, Rev. Mod. Phys. **56**, 755 (1984).
[3] N. Grewe and F. Steglich, in *Handbook on the Physics and Chemistry of Rare Earths* (North-Holland, Amsterdam, 1991), Vol. 14.
[4] P. Fulde, J. Keller, and G. Zwicknagl, in *Solid State Physics* (Academic, New York, 1988), Vol. 41.
[5] H. R. Ott, in *Progress in Low Temperature Physics* (North-Holland, Amsterdam, 1987), Vol. 9.
[6] R. Citro, A. Romano, and J. Spałek, Physica B (Amsterdam, Neth.) **259–261**, 213 (1999).
[7] I. Sheikin, A. Gröger, S. Raymond, D. Jaccard, D. Aoki, H. Harima, and J. Flouquet, Phys. Rev. B **67**, 094420 (2003).
[8] A. McCollam, S. R. Julian, P. M. C. Rourke, D. Aoki, and J. Flouquet, Phys. Rev. Lett. **94**, 186401 (2005).
[9] R. Doradziński and J. Spałek, Phys. Rev. B **56**, R14239 (1997).
[10] R. Doradziński and J. Spałek, Phys. Rev. B **58**, 3293 (1998).
[11] C. Pfleiderer, Rev. Mod. Phys. **81**, 1551 (2009).
[12] G. R. Stewart, Rev. Mod. Phys. **73**, 797 (2001).
[13] H. v. Löhneysen, A. Rosch, M. Vojta, and P. Wölfle, Rev. Mod. Phys. **79**, 1015 (2007).
[14] G. Lonzarich, Nat. Phys. **1**, 5 (2005).
[15] C. Lacroix and M. Cyrot, Phys. Rev. B **20**, 1969 (1979).
[16] A. C. Hewson, *The Kondo Problem to Heavy Fermions* (Cambridge University Press, Cambridge, 1993).
[17] A. Auerbach and K. Levin, J. Appl. Phys. **61**, 3162 (1987).
[18] O. Howczak and J. Spałek, J. Phys. Condens. Matter **24**, 205602 (2012).
[19] O. Howczak, J. Kaczmarczyk, and J. Spałek, Phys. Status Solidi B **250**, 609 (2013).
[20] P. Gurin and Z. Gulácsi, Phys. Rev. B **64**, 045118 (2001).
[21] Z. Gulácsi, Phys. Rev. B **66**, 165109 (2002).
[22] Z. Gulácsi and D. Vollhardt, Phys. Rev. Lett. **91**, 186401 (2003).
[23] Z. Gulácsi and D. Vollhardt, Phys. Rev. B **72**, 075130 (2005).
[24] C. M. Varma, W. Weber, and L. J. Randall, Phys. Rev. B **33**, 1015 (1986).
[25] Z. Gulácsi, R. Strack, and D. Vollhardt, Phys. Rev. B **47**, 8594 (1993).
[26] T. M. Rice and K. Ueda, Phys. Rev. Lett. **55**, 995 (1985).
[27] T. M. Rice and K. Ueda, Phys. Rev. B **34**, 6420 (1986).
[28] K. Miyake, S. Schmitt-Rink, and C. M. Varma, Phys. Rev. B **34**, 6554 (1986).
[29] P. Fazekas, *Electron Correlation and Magnetism* (World Scientific, Singapore, 1999).
[30] G. Kotliar and A. E. Ruckenstein, Phys. Rev. Lett. **57**, 1362 (1986).
[31] J. Spałek, A. Datta, and J. M. Honig, Phys. Rev. Lett. **59**, 728 (1987).
[32] F. Gebhard, Phys. Rev. B **44**, 992 (1991).
[33] V. Dorin and P. Schlottmann, Phys. Rev. B **46**, 10800 (1992).
[34] V. Dorin and P. Schlottmann, Phys. Rev. B **47**, 5095 (1993).
[35] J. Bünemann, W. Weber, and F. Gebhard, Phys. Rev. B **57**, 6896 (1998).
[36] J. Jędrak and J. Spałek, Phys. Rev. B **83**, 104512 (2011).
[37] J. Kaczmarczyk and J. Spałek, Phys. Rev. B **84**, 125140 (2011).
[38] M. Abram, J. Kaczmarczyk, J. Jędrak, and J. Spałek, Phys. Rev. B **88**, 094502 (2013).
[39] A. P. Kądzielawa, J. Spałek, J. Kurzyk, and W. Wójcik, Eur. Phys. J. B **86**, 252 (2013).
[40] M. Zegrodnik, J. Bünemann, and J. Spałek, New J. Phys. **16**, 033001 (2014).
[41] M. M. Wysokiński and J. Spałek, J. Phys. Condens. Matter **26**, 055601 (2014).
[42] M. M. Wysokiński, M. Abram, and J. Spałek, Phys. Rev. B **90**, 081114(R) (2014).
[43] M. M. Wysokiński, M. Abram, and J. Spałek, Phys. Rev. B **91**, 081108(R) (2015).
[44] B. Edegger, V. N. Muthukumar, and C. Gros, Phys. Rev. B **74**, 165109 (2006).
[45] M. Lugas, L. Spanu, F. Becca, and S. Sorella, Phys. Rev. B **74**, 165122 (2006).
[46] M. Raczkowski, M. Capello, D. Poilblanc, R. Frésard, and A. M. Oleś, Phys. Rev. B **76**, 140505 (2007).
[47] B. Edegger, V. N. Muthukumar, and C. Gros, Adv. Phys. **56**, 927 (2007).
[48] C.-P. Chou, F. Yang, and T.-K. Lee, Phys. Rev. B **85**, 054510 (2012).
[49] J. Liu, J. Schmalian, and N. Trivedi, Phys. Rev. Lett. **94**, 127003 (2005).
[50] T. Watanabe, H. Yokoyama, K. Shigeta, and M. Ogata, New J. Phys. **11**, 075011 (2009).
[51] M. Z. Asadzadeh, F. Becca, and M. Fabrizio, Phys. Rev. B **87**, 205144 (2013).
[52] H. Watanabe, K. Seki, and S. Yunoki, Phys. Rev. B **91**, 205135 (2015).

[53] R. Jastrow, Phys. Rev. **98**, 1479 (1955).
[54] J. Bünemann, T. Schickling, and F. Gebhard, Europhys. Lett. **98**, 27006 (2012).
[55] J. Kaczmarczyk, J. Spałek, T. Schickling, and J. Bünemann, Phys. Rev. B **88**, 115127 (2013).
[56] J. Kaczmarczyk, J. Bünemann, and J. Spałek, New J. Phys. **16**, 073018 (2014).
[57] J. Kaczmarczyk, Philos. Mag. **95**, 563 (2015).
[58] J. Kaczmarczyk, T. Schickling, and J. Bünemann, Phys. Status Solidi B (2015), doi:10.1002/pssb.201552082.
[59] P. Aynajian, E. H. da Silva Neto, A. Gyenis, R. E. Baumbach, J. D. Thompson, Z. Fisk, E. D. Bauer, and A. Yazdani, Nature (London) **486**, 201 (2012).
[60] M. P. Allan, F. Massee, D. K. Morr, J. S. Dyke, A. W. Rost, A. P. Mackenzie, C. Petrovic, and J. C. S. Davis, Nat. Phys. **9**, 468 (2013).
[61] J. S. Dyke, F. Massee, M. P. Allan, J. C. S. Davis, C. Petrovic, and D. K. Morr, Proc. Natl. Acad. Sci. USA **111**, 11663 (2014).
[62] A. T. Holmes, D. Jaccard, and K. Miyake, Phys. Rev. B **69**, 024508 (2004).
[63] A. Ślebarski and J. Spałek, Phys. Rev. Lett. **95**, 046402 (2005).
[64] A. Ślebarski, J. Spałek, M. Fijałkowski, J. Goraus, T. Cichorek, and L. Bochenek, Phys. Rev. B **82**, 235106 (2010).
[65] M. Szlawska, D. Kaczorowski, A. Ślebarski, L. Gulay, and J. Stępień-Damm, Phys. Rev. B **79**, 134435 (2009).
[66] D. Kaczorowski and A. Ślebarski, Phys. Rev. B **81**, 214411 (2010).
[67] S. Watanabe and K. Miyake, Phys. Rev. Lett. **105**, 186403 (2010).
[68] H. Tsunetsugu, M. Sigrist, and K. Ueda, Rev. Mod. Phys. **69**, 809 (1997).
[69] In principle, the hybridization can have an intersite character [83].
[70] F. Gebhard, Phys. Rev. B **41**, 9452 (1990).
[71] Z. Gulácsi, M. Gulácsi, and B. Jankó, Phys. Rev. B **47**, 4168 (1993).
[72] A. L. Fetter and J. D. Walecka, *Quantum Theory of Many-Particle Systems* (Dover, New York, 2003).
[73] M. Galassi, J. Davies, J. Theiler, B. Gough, G. Jungman, P. Alken, M. Booth, and F. Rossi, GNU Scientific Library Reference Manual, 3rd ed., https://www.gnu.org/software/gsl/manual/html_node/Further-Information.html.
[74] K. Miyake and Y. Onishi, J. Phys. Soc. Jpn. **69**, 355 (2000).
[75] J. Spałek, Philos. Mag. **95**, 661 (2015).
[76] S. Doniach, Phys. Rev. B **35**, 1814 (1987).
[77] B. Coqblin, C. Lacroix, M. A. Gusmão, and J. R. Iglesias, Phys. Rev. B **67**, 064417 (2003).
[78] S. Hoshino and Y. Kuramoto, Phys. Rev. Lett. **111**, 026401 (2013).
[79] T. Park, M. J. Graf, L. Boulaevskii, J. L. Sarrao, and J. D. Thompson, Proc. Natl. Acad. Sci. USA **105**, 6825 (2008).
[80] R. Troć, Z. Gajek, and A. Pikul, Phys. Rev. B **86**, 224403 (2012).
[81] M. M. Wysokiński, J. Kaczmarczyk, and J. Spałek (unpublished).
[82] J. Jçdrak, J. Kaczmarczyk, and J. Spałek, arXiv:1008.0021.
[83] P. Ghaemi, T. Senthil, and P. Coleman, Phys. Rev. B **77**, 245108 (2008).